Effect of Caribbean Water Incursion into the Gulf of Mexico derived from Absolute Dynamic Topography, Satellite Data, and Remotely - sensed Chlorophyll-*a*

Authors:

Juan A. Delgado[1,2,5]**; Joël Sudre** [3]**, Sorayda Tanahara**[1]**; Ivonne Montes**[4]**,**

J. Martín Hernández-Ayón[5]**, Alberto Zirino**[6]

Author affiliations:
[1]*Facultad de Ciencias Marinas, Universidad Autónoma de Baja California, Transpeninsular Tijuana-Ensenada, no. 3917, Fraccionamiento Playitas, CP 22860. Ensenada, Baja California, México.*
[2]*Instituto Tecnológico de Guaymas/ Tec. Nacional de México, Guaymas, Sonora, México.*
[3]*LEGOS, CNRS/IRD/UPS/CNES UMR 5566, 18 av. Ed Belin, 31401 Toulouse Cedex 9, France*
[4]*Insitituto Geofísico del Perú. Lima, Perú.*
[5]*Instituto de Investigaciones Oceanológicas, Universidad Autónoma de Baja California, Transpeninsular Tijuana-Ensenada, no. 3917, Fraccionamiento Playitas, CP 22860. Ensenada, Baja California, México.*
[6]*Scripps Institution of Oceanography, University of California, San Diego, 9500 Gilman Drive, La Jolla, California 92093, USA.*
Corresponding author: Sorayda Tanahara (stanahara@uabc.edu.mx)
Facultad de Ciencias Marinas
Universidad Autónoma de Baja California.

Key points:

Twenty-five years of satellite observations of absolute dynamic topography confirm the patterns

of Caribbean water intrusion in the Gulf of Mexico.

Larger volumes of oligotrophic waters from Caribbean Sea are entering the western Gulf of

Mexico and lowering the surface and near surface *Chl-a* concentration.

Abstract

The dynamics of the Loop Current (LC) and the detached Loop Current eddies (LCEs) dominate the surface circulation of the Gulf of Mexico (GoM) and transport Caribbean water (CW) into the gulf. In this work, 25-years (1993-2017) of daily satellite data are used to investigate the variability of these physical processes and their effect on chlorophyll-a (Chl-a) concentrations from 1998-2017 including temporal changes, mean differences, and regional concentration tendencies. Physical variables analyzed are absolute dynamic topography (ADT), oceanic currents, and wind stress. From the ADT and oceanic current monthly climatologies, it is shown that there is an annual intrusion of the CW with an inward incursion that starts in spring, peaks in the summer, reaches to 28°N and 90.45°W, and then retreats in winter to 26.5 °N and 88.3 °W, approximately. Minimum surface Chl-a concentrations (<0.08 mg m^{-3}) are found during the summer-autumn period inside the region of maximum incursion of the CW; the opposite is observed during the winter period when Chl-a concentrations were at a maximum, e.g., >0.14 mg m^{-3}. The three-year running averages of the ADT 40-cm isoline reproduce qualitatively the climatological pattern of 25 years showing that before 2002 the CW was less intrusive. This suggests that from 2003 onward, larger volumes of oligotrophic waters from Caribbean Sea have invaded the western GoM and reduced mean surface Chl-a concentrations. A direct comparison between the 1998-2002 and 2009-2014 periods indicates that in the latter time interval, Chl-a concentration above waters deeper than 250 m has decreased significantly.

1. Introduction

The effects of global warming on the circulation of the world's oceans and its concomitant consequences on the oceans' biological productivity are some of the most important scientific and economic issues of our times. Forecasting of the effects of global warming on the oceans' resources

58 depends on having a clear understanding of the manner in which physical processes (e.g., solar

59 radiation, winds, circulation and vertical mixing) affect primary production. This understanding is

60 aided by the availability of remote sensing observations, unparalleled in their spatial and temporal

61 coverage of the earth's surface. Since 1990, satellite data of absolute dynamic heights (ADT),

62 Chlorophyll-a (Chl-a) concentration, and derived products (eddy kinetic energy (EKE),

63 geostrophic and Ekman currents) have been available to study the Gulf of Mexico (GoM), an

64 important socio-economic region for fisheries, petroleum, natural gas, and tourism. We have

65 availed ourselves of a 25-year time series of satellite data to study the relationship between the

66 physical dynamics of the GoM and its effect on primary production in the context of a global

67 warming scenario. Unlike previous studies, this work entails the analysis of the Loop Current (LC)

68 and the LC eddies (LCEs) path footprint, and of the dominant features of the surface circulation

69 that transport Caribbean Water (CW) into the GoM (Nowlin and McLellan, 1967; Morrison et al.,

70 1983). The LC in the eastern GoM is part of the North Atlantic Ocean Subtropical Gyre, an

71 essential contributor to the inter-hemispheric Meridional Overturning Cell (Schmitz and

72 McCartney, 1993; Candela et al., 2003; Schmitz et al., 2005). This current carries warm waters

73 from the gulf to the North Atlantic through the Florida Straits via the Gulf Stream (Hurlburt and

74 Thompson, 1980), thereby also being an important contributor to the upper ocean heat budget of

75 GoM (Liu et al., 2012). Based on a detailed analysis in the central and western GoM by Portela et

76 al. (2018), within the Gulf are seven water masses in order of increasing mean density: remnants

77 of the Caribbean Surface Water (CSWr: also referred to as CW), North Atlantic Subtropical

78 Underwater (NASUW), Gulf Common Water (GCW), Tropical Atlantic Central Water (TACW),

79 the nucleus of the (TACWn), Atlantic Intermediate Water (AAIW) and North Atlantic Depth

80 Water (NADW). Here, we are principally concerned with surface effects.

81   CW enters in the GoM via the LC with specific biological (i.e., low Chl-a) and physical

82   characteristics (warmer and more saline waters). The current penetrates into the gulf, reaching

83   28˚N, near the Mississippi Delta. As it extends to the north, it forms a loop (Austin, 1955) that

84   turns southeast to ultimately exit into the Atlantic Ocean.

85   Knowledge of how the thrust of the LC affects the intrusion of CW is based on

86   hydrographic data (Leipper, 1970; Niiler 1976; Behringer et al., 1977; Molinari et al., 1977; Huh

87   et al., 1981; Paluszkiewicz et al., 1983), remote sensing observations (Vukovich et al.1979;

88   Vukovich, 1988; Leben and Born, 1993; Leben, 2005), and, in the last twenty years, by numerical

89   modeling (Hurlburt and Thompson, 1980; Candela et al., 2003; Oey et al., 2005; Sturges and Lugo-

90   Fernandez, 2005; Counillon and Bertino, 2009; Cardona and Bracco, 2016; Wei et al., 2016). More

91   recently, novel developments based on artificial neural networks and empirical orthogonal

92   function analysis have also been applied to predict LC variation (Zeng et al., 2015), effecting

93   reliable forecasts for up to 5 to 6 weeks. Knowledge of how the primary forcing mechanism affects

94   the loop current is important to the circulation of the GoM both as a direct and indirect generator

95   of surface-layer eddies and as a source of lower-layer flows (Hamilton et al., 2016). Based on

96   satellite altimetry observations and the dynamic height gradient from 1993 to 2009, Lindo-Atichati

97   et al. (2013) observed northward seasonal penetration of the LC, peaking in summer. LC extension

98   and anticyclonic eddy separation are the result of the momentum imbalance (Pichevin and Nof,

99   1997) and form the shape of future LCEs. Chang and Oey (2010) using a numerical model,

100   proposed that the wind stress could be the primary forcing that releases LCEs. In a second paper,

101   supported by satellite observations, they proposed that the LC intrusion and the shedding of the

102   LCEs followed a biannual cycle (Chang and Oey, 2013). A reanalysis of archived data also

103   detected statistically significant LCEs separation seasonality (Hall and Leben, 2016). Recently,

104 Candela et al. (2019) analyzed four years of water current data and reported a seasonal cycle in the

105 transport through the Yucatan channel with the annual cycle as the main harmonic peak in July.

106 Interacting seasonal and stochastic processes could trigger the separation of the LCEs

107 (Fratantoni et al., 1998; Zavala-Hidalgo et al., 2003; Zavala-Hidalgo et al., 2006) as well as

108 forming Caribbean eddies and other topographic features (Garcia-Jove et al., 2016). In this context,

109 the LC system has some similarities with the North Brazil Current retroflection (Pichevin et al.,

110 1999; Goni and Johns, 2001; Zharkov and Nof, 2010), the Agulhas retroflection (de Ruijter et al.,

111 1999; Baker-Yeboah et al., 2010) and with the Gulf Stream, where large meanders pinch off as

112 warm rings (Brown et al., 1983; Richardson, 1983; Savidge and Bane, 1999).

113 Despite extensive research, after more than a half-century we are still struggling to

114 completely understand LC variability, the processes controlling the loop current extension, and the

115 mechanism of detachment of anticyclones from the loop. Because positive time trends have been

116 reported in temperature, winds, sea level and the greater number of detached eddies separated from

117 the LC, it can be expected that these phenomena would affect primary productivity and, indirectly,

118 surface Chl-a concentration (Polovina, et al., 2008; Laffoley and Baxter., 2016). In this work, 25-

119 years (1993-2017) of daily ADT data combined with monthly radiance data from 1998-2017 are

120 used to investigate the variability of the transport of Caribbean surface water into the gulf and its

121 effect on Chl-a concentration. We examined temporal changes, mean differences, and regional

122 concentration tendencies.

123

124 **2. Data and Methods**

125 Three independent data sets were used to provide evidence of temporal variability in the extension

126 of CW into the GoM. We used ADT and surface velocity fields (geostrophy and Ekman) from the

127 GEKCO (Geostrophic Ekman Current Observatory, Sudre et al., 2013) product from 1993 - 2017

128 with a resolution of 0.25˚x0.25˚, in conjunction with *Chl-a* ocean color data derived from the

129 reprocessing R2014.0 product suite from Aqua MODIS (Moderate Resolution Imaging

130 Spectroradiometer) and from SeaWIFS (Sea-Viewing Wide Field of view Sensor), using the OCx

131 Algorithm with a spatial resolution of 9X9 km (https://oceancolor.gsfc.nasa.gov/cgi/l3). The 2003-

132 2017 monthly *Chl-a* ocean color product was derived from Aqua MODIS and the 1998-2002

133 monthly *Chl-a* ocean color product was derived from SeaWIFS.

134 Climatology was created from maps of ADT that result from the elevation of the sea surface

135 height referenced to the geoid using the product from DUACS (Data Unification and Altimeter

136 Combination System) available on the AVISO (Archiving, Validation and Interpretation of

137 Satellite Oceanographic data) website https://www.aviso.altimetry.fr/en/data. The ADT

138 climatology was constructed using the 25 years of daily satellite maps, from 1993 to 2017,

139 averaging all the Januaries, Februaries … and Decembers. We considered LCEs in any stage of

140 formation, detaching and reattaching to the LC as evidence of the incursion of the CW. After the

141 ADT climatology was obtained, the predominant boundary contour of CW was extracted from

142 each climatological month. It was observed that the 40 ±2.2 cm ADT contour was well matched

143 to the climatological maxima of its respective EKE. For this reason, the ADT 40 cm contour is

144 taken as the main ADT reference that tracks the Caribbean Water Front (CWF).

145 Specifically, monthly CWF positions were obtained from short-term running averages of

146 daily satellite observations in three-year periods. Each running average was moved rearward by

147 one year, e.g. 1993-1995, 1994-1996 … 2014-2016, 2015-2017. For each three-year period, a set

148 of 12 monthly maps was obtained resulting in a total of 23 sets of monthly CWF maps: 10 sets

149 from 1993 to 2002 and 13 sets from 2003 to 2017. We used the 40 cm contour of each set of three-

150   year averages because this was the contour with the highest EKE observed in the 25-year data set.

151   To retrieve the CWF contours, we first determined the initial latitudinal position of the CWF to be

152   at 80.7ºW with the respective corresponding longitudinal positions between Cuba and Florida. The

153   CWF contour lines that run from east to west and finish close to the tip of the Yucatan peninsula

154   were separated by 0.2 ±0.1 degrees. However, some ADT contour "islands" appeared next to the

155   CWF with a typical distance of > 0.3 degrees from the CWF contour. Additionally, a spectral

156   analysis was done using a daily time series of 25 years of ADT data to build a spatially averaged

157   region influenced by the LC between 91.25ºW, 23.125ºN and 83.5ºW, 28.12ºN.

158   When ADT island distances were > 0.3 degrees from the front, we used a Matlab code

159   procedure to eliminate them from the CWF contours. Once the CWF's contours were retrieved, the

160   next step was to visually corroborate the quality and coherence of each CWF contour over the

161   monthly field maps of ADT, sea surface currents, and *Chl-a* distribution. In this way,

162   inconsistencies were detected and corrected. The Matlab code procedure satisfactorily corrected

163   91.3% of the contours. The remaining sets were corrected by hand via visual analysis.

164   Main mesoscale instabilities were obtained from calculations of the climatological monthly

165   EKE maps of geostrophic and Ekman currents obtained from 25 years of daily satellite

166   observations of GEKCO using following equation:

167   $$u = u' + U; \qquad u' = u - U$$

168   $$v = v' + V; \qquad v' = v - V$$

169   $$EKE = \tfrac{1}{2}\,(u'^2 + v'^2)$$
170
171   Where (u, v) is the total current ($u = u_E + u_g$ and $v = v_E + v_g$; (u_E, v_E), is the Ekman and (u_g, v_g) is the

172   geostrophic current, U and V are the means of the oceanic currents and (u' and v') are the anomalies

173   of the current. To find the relationship between ADT and EKE patterns, the 40 *cm* ADT isoline

174   was overlaid on the monthly EKE maps. This made the EKE means representative of the energy

175   of the mesoscale eddy field (Jouanno et al., 2012).

176   For consistency between the different satellite datasets, all monthly climatological spatial

177   fields were standardized at 0.25˚x0.25˚ spatial resolution by bilinear interpolation.

178

3. Results and discussion

3.1. Tracking the Intrusion of Caribbean Water

181   The LC enters the gulf through the Yucatan Channel and exits through the Straits of Florida,

182   penetrating northward into the GoM until instabilities form in the current and a ring-like LCEs

183   pinches off. There are two ways of tracking the LC: 1) tracking the thermal signal (not possible in

184   summer due to weak thermal contrast in the GoM), and 2) tracking the sea surface height trough

185   the satellite altimetry. In 2005, Leben, using the 17 *cm* contour in the daily sea surface topography

186   maps (this contour closely follows the edge of the high-velocity core of the LCEs and LC), tracked

187   the LC thermal fronts in the sea surface temperature images during good thermal contrast. In a

188   different way, Lindo-Atichati et al. (2013) calculated the maximum horizontal gradient of the sea

189   surface height (SSH) to track only the contours of the LCF. In this work, we used the ADT to track

190   both the LC and the LCEs formed by the influence of the CW. Monthly mean surface oceanic

191   currents from GEKCO overplotted on the ADT data are shown in Fig. 1. Maximum satellite

192   surface current velocities in the Caribbean Sea and the GoM, as well as in the Yucatan current on

193   the continental coast, were > 50 *cm s^{-1}*, coinciding with *in situ* estimates of ~ 60 *cm s^{-1}* (Badan et

194   al., 2005). The monthly GoM total current fields show the variability of the primary forcing that

195   coincides with the mean ADT edge; the vectors of maximum velocity are tangent to the edge of

196   the maximum slope change. To locate the CW, the 40 *cm* mean ADT's isoline was chosen. The

197   ADT reference corresponds to regions of maximum gradients of ADT and maximum EKE. Fig. 1

198   shows that (mostly) in autumn (October, November and December) and winter (January, February

199   and March), the CW retracts to its most southeasterly location. In contrast, in spring (April, May,

200   June) and summer (July, August, September), CW penetration moves towards the northwest. In

201   fact, the extension begins in May and reaches maximum penetration in August, showing an annual

202   pattern. This movement is similar to that observed by Chang and Oey (2013). They found that in

203   summer, the maximum LC intrusion was forced by the trade winds. Their and our observations

204   are also consistent with the work of Candela et al. (2019) who reported that water transport into

205   the GoM in July through the Yucatan channel was at a maximum.

206   It is accepted that the LCEs occur in a geographical control zone that is based on

207   momentum imbalance (Pichevin and Nof, 1997; Nof, 2005) rather than instability. Also, we should

208   not abandon the idea that the formation of instabilities such as meanders and cyclonic eddies are

209   due to high EKE produced by upstream conditions that influence the circulation within the GoM

210   (Oey et al., 2003) and produce changes in the fluxes in the Yucatan Channel (Candela et al., 2002),

211   transport variations in the LC (Maul and Vukovich, 1993), variations in the deep outflow (Bunge

212   et al., 2002), and cyclonic eddies in Campeche Bank and Tortugas (Fratantoni et al., 1998; Zavala-

213   Hidalgo et al*.,* 2003). The areas of large EKE are related to the intrusion and retreat of CW (Garcia-

214   Jove et al., 2016) via baroclinic and barotropic instabilities (e.g. Jouanno et al*.,* 2009).

215   Fig. 2 shows that the 40 *cm* isoline encloses the maximum EKE area of the LC-LCEs during

216   each climatological month, demonstrating that its distribution is mainly centered in the LC region;

217   consequently, the maximum EKE borders the CW front just where the abrupt horizontal gradients

218   of ADT exist and changes of current speed occur. It is clear that the 40 *cm* isoline of ADT matches

219   very well both the maximum EKE values and the maximum ADT gradient and is a good tracker

220   of the contours of LC-LCEs. Lindo-Atichati et al. (2013) proposed a methodology using the SSH

221   maximum horizontal gradient, which is the addition of sea height anomaly and mean dynamic

222   topography, to obtain the contours of LCF and the LCEs. In our analysis, we chose the 40 *cm*

223   isoline as a general reference to track both LCF and LCEs, and CW transport.

224   The enhanced monthly EKE signals respond in the same way as the LCF, repeating the

225   mean monthly pattern as well as the total currents; the CW intrusion starts in spring and peaks in

226   summer to retract in autumn and winter, and there are no relevant mesoscale EKE's structures in

227   the western GoM. These results confirm an annual pattern of CW intrusion in summer months and

228   retraction in winter.

229   **3.2 West and Northward Caribbean water extension**

230   The monthly intrusions of the CWF were tracked by taking as a reference the northernmost

231   latitudes and westernmost longitudes of the 40 *cm* ADT isoline representing 1993-2017 monthly

232   average values of the ADT (not spatially averaged). The climatological position of the CWF for

233   each month of the year is shown in Figure 3. These results confirm the annual intrusion of the CW

234   as follows: 1) Analysis of the maximum north and westward penetration of the front over 25 years

235   shows that from January to February, it is retracted southeast to ~ 26.55°N and ~ 88.32°W (Fig. 3a

236   and 3b, respectively), and intrudes to 28°N, 90.45°W in August; 2) an ADT spectral analysis

237   derived from 25 years of daily data from the CWF region shows a strong annual signal that

238   originates from the back and forth of the ADT signal (Fig. 3c). In this work, the ADT signal also

239   includes the seasonal steric effect. Based on Hall and Leben (2016), a steric signal appears as an

240   annual sine wave with 5.8 cm amplitude. When the estimated seasonal steric influence is removed,

241   the high energy peak diminishes by 74%.

242   In winter, the "tongue" of the CWF moves slowly to the north without westward advance;

243   in spring it lengthens and travels slightly towards the west. From January to March, the northward

244   CWF position shifts slowly, tracing a gently sloping line, that starts at 26.5˚N, reaches its

245   maximum northern position of 28˚N in August, and then decreases in December to 26.28˚N

246   (maximum travel of the CWF was 1.72˚ or 191 *km)*. In summer, the CWF intrudes further into the

247   interior of the GoM both in the north and west: its maximum northern and westward advance

248   occurs in August to 28˚N and 90.45˚W, but then the CWF retracts in the last month of summer.

249   Regarding CWF´s westerly movement (Fig. 3b), the CWF traveled little from January to April; in

250   May however, it extended quickly and in July, August, and September reached approximately

251   90.2˚W, and peaked in October at 90.76 ˚W (maximum range was 2.56˚ or 253 *km,* calculated at

252   27.5˚N latitude). In December, the CWF retracted abruptly to 88.24˚W.

253   Another aspect of the CWF is the rate of intrusion and retraction. From March to August,

254   the CWF moves to the north with a penetration speed on the order of ~ 1.02 *km day^{-1}*, covering a

255   distance of 153 *km or* 1.37˚. On the other hand, the rate of retraction from August to November is

256   ~ 1.86 *km day^{-1},* equivalent to *168 km (1.51˚).* The entire process of northerly intrusion occurred

257   in three stages: first, from January to April, the front moved slowly northward, increasing its speed

258   while maintaining its westward position. Between May and July the front moved northwest; then

259   was quasi-stationary in July and August, near 90.45˚W; finally, in September, it moved from

260   90.13˚W to 90.76˚W, equivalent to 63 *km* at a rate of 2.1 *km day^{-1}*. The retraction to the west

261   occurred relatively quickly as the front retracted 193 *km* towards the east in a single month

262   (October) at the rate of 6.3 *km day^{-1}*, and in November traveled 41 *km* at a rate of 1.4 *km day^{-1},*

263   also towards the east.

264   Fig. 4 shows the calculated climatological areas of standard deviation (STD) of the CWF

265   contours > 15 cm (dotted line) and CWF contours > 40 cm (heavy black line). From these areas

266   we calculated ratios between the two (15cm/40cm). The STD contour of 15 cm was selected

267   because this value was three times greater than the annual steric signal reported by Hall and Leben

268   (2016). Ratio values greater than 1 were found in February (1.62) and April (1.60). From May to

269   August, the monthly ratio descended to 1.36, , and increased in September back to 1.60, peaking

270   in October to 1.68, then decreasing in November to 1.60 and finally settling to 1.62 in December.

271   The average winter months (Dec., Jan., and Feb.) had an average ratio of 1.56. From March to

272   July, The average ratio was 1.40. However, in August the ratio increased abruptly to 1.60. Fall

273   (Sept., Oct., and Nov.) had high ratios, averaging 1.62. Chang and Oey (2012, 2013) proposed that

274   the LC intrusion and the shedding of the LCEs followed a biannual cycle. The biannual cycle can

275   also be related to the annual lowest and highest ratio values.

276   **3.3 Monthly Spatial Variability of the Caribbean Water Front**

277   It was found that where penetration-retraction of the CWF occurs, STD variability varies from 15

278   to 35 *cm*, extending west to 90.8°W in winter and 93.5°W in summer (Fig. 4). West of the CWF,

279   in the deep zone of the GoM, the observed variability was close to 10 *cm* distributed in the band

280   of latitude between 23°N and 28.5°N. The regions of maximum variability (STD > 15 *cm*) occur

281   in the CWF zone and extend outside the irregular area of reference (isoline of the 40 *cm* ADT).

282   The effect of CWF penetration and regions of anticyclonic circulation was determined from the

283   area of the variability of ADT, with maximum values close to ~35 *cm* in the central region of the

284   CWF, at 86.67°W and 25.6°N. The percentage of the area of influence of STD > 15 *cm* in relation

285   to the area of the gulf (1.56×10^6 *km²*) is presented in Fig. 5, where a gradual monthly increase is

286   observed from January to October, followed by a decrease in November and December. In January,

287   the direct influence of the CWF on the gulf by area was 12.4%, rising to 21.5% for October, to

288   subsequently decrease in December to 15.4%. We suppose that the greater percentage area of the

289   STD may be attributed to a greater influence of Caribbean Sea water.

290   **3.4 Changes in the Caribbean Water Incursion from 2003 to the Present**

291   Using the 40 *cm* reference, a 3-year running average of the ADT data was calculated to extract the

292   minimum number of years that would produce a similar pattern over a quarter century of the CWF.

293   The results indicate a difference in CWF path and westward penetration before and after 2002. It

294   is observed that before 2002 the CWF was less intrusive in the west (Fig. 6), after 2002 it extended

295   towards the west in both summer and autumn (Fig. 7). It is important to note that the intrusion of

296   the CWF is due to the influence of LCEs that have a strong presence in the western GoM. This

297   fact is supported by a statistical analysis of the lifetimes of the LCEs during two time periods

298   (1993-2002 and 2003-2015) (http://www.horizonmarine.com/loop-current-eddies.html). The data

299   shows that the LCEs in the 1993-2002 period had a mean life of 6.8 months while the average life

300   in 2003-2015 was 11.7 months. To prove that there is significant difference between these periods,

301   a student-*t* test was applied with the result that the difference between them is significant (t = -

302   3.098, p = 0.005). The LCE mean life difference is clear evidence that the incoming volume of

303   water from Caribbean Sea (with oligotrophic features, Aguirre –Gómez and Salmerón-García,

304   2015) has reached farther in the western GoM after 2002. These observations also agree with the

305   results of Lindo-Atichati et al. (2013), confirming that, on average, the LC northward intrusion

306   starts to increase in 2002. These authors also report an increase in number/year of LC rings over

307   the same period that also coincided with a significant increase in sea height residuals (2.78 ± 0.26

308   cm/decade from 1993–2009). This supports the finding that from 2003 onward, larger volumes of

309   oligotrophic waters from Caribbean Sea have invaded the western GoM.

310   **3.5 Chlorophyll-a Satellite Imagery, Climatology, and Changes in the Last Decade**

311   Another product that tracks the effect of CW inside the western GoM is the *Chl-a* satellite imagery,

312   being an index of primary productivity (Boyer et al., 2009). Physical processes that affect the

313   distribution and abundance of *Chl-a* include estuarine influxes, depth of the nutricline, wind stress,

314   thermal stratification and eddy advection. However, over deep waters of the GoM, it is the wind

315   stress and the thermal stratification that principally affect the *Chl-a* concentration (Martínez-López

316   and Zavala-Hidalgo, 2009; Müller-Karger et al., 2015, Damien et al., 2018). It was found that the

317   oligotrophic CW contrasts seasonally with the gulf waters and allows the observation of two levels

318   of *Chl-a* (high and low, Müller-Karger et al., 1989). Here, the temporal relationship between the

319   CWF and *Chl-a* concentration was constructed from SeaWifs and MODIS monthly climatological

320   images (Fig. 8). The highest concentrations of *Chl-a* in the interior of the GoM are observed during

321   autumn and winter months when high concentrations are triggered by vertical mixing (Pasqueron

322   de Fommervault et al., 2017; Damien et al., 2018) when values were > 0.14 *mg m^{-3}* in agreement

323   with Dandonneau et al. (2004), whereas in spring-summer they decreased to 0.08 - 0.09 *mg m^{-3}*.

324   During spring-summer, when the maximum CW penetration occurs, our data confirms that the

325   "footprint" of the CWF water (delineated by the 40 *cm* isoline of ADT) is in general oligotrophic

326   indicating that Caribbean water has indeed entered the GoM. During this period, the *Chl-a* surface

327   concentration remains low as the increase in surface temperature strengthens stratification.

328   Additionally, the winds from the southeast are weak, thereby reducing the mixing of nutrients to

329   the surface. In contrast, during the autumn-winter months, the northerly winds are stronger,

330   increasing vertical mixing, deepening the mixed layer, and carrying cold, nutrient-rich subsurface

331   water into the euphotic layer (Müller-Karger et al., 1991; Müller-Karger et al., 2015; Pasqueron

332   de Fommervault et al., 2017).

333   In seeking relationships between the spatial-seasonal distribution of the *Chl-a*

334   concentration and the incursion signaled by the ADT-generated data, three spatial-temporal

335   periods were selected, each was averaged pixel by pixel, and the three were labeled: "early" (1998-

336   2002), "middle" (2003-2008), and "contemporary" (2009-2014) epochs. The 5-year averages of

337   the "early" and "contemporary' periods of two separate areas were compared: 1) an area located in

338   the western GoM at 95.5˚W, 22.12˚N and 91.5˚W, 25.87˚N, and 2) a smaller area located in the

339   center of the LC at 86˚W, 22.12˚N and 84.75˚W, 23.37˚N (Fig. 9). The differences in the means

340   were tested for significance with a 2-tailed z test at the 95% confidence level (Fowler et al., 2013).

341   The results are shown in Table 1 and may be summarized as follows:

342   **A**. Temporal differences: 1) Western GoM differences between early and contemporary *Chl-a*

343   concentrations are significantly different in all seasons; 2) Loop Current differences between Early

344   and Contemporary *Chl-a* concentrations are significantly different during winter, spring, and

345   autumn, but not in summer;

346   **B**. Spatial differences: 1) In winter, the Western GoM is significantly higher in *Chl-a* than the LC

347   during both early and contemporary periods; 2) In the spring, the Western GoM is significantly

348   higher than the LC during the early period, but not in contemporary period; 3) In summer, the LC

349   is significantly higher than Western GoM during both early and contemporary periods; 4) In

350   autumn, the Western GoM is significantly higher than LC during the "early" period but not

351   significantly different from the LC in the contemporary period.

352   **C**. Seasonal Differences. In the Western GoM and the LC in both the early and contemporary

353   periods, *Chl-a* decreases from winter to spring and from spring to summer, and increases from

354 autumn to winter, but autumn concentrations do not exceed winter (See also Fig.9). All differences

355 are significant.

356   Examination of Table 1 indicates that at both areas, the winter season is most productive,

357 followed by autumn, with the lowest *Chl-a* concentrations occurring in summer (see also Fig. 9).

358 There is also a time-dependent trend, with contemporary values that are, in general, lower than the

359 values in the early and middle epochs. Both areas exhibit identical climatic trends over time and

360 during each season, indicating that these effects are applicable outside of the continental shelf. The

361 early spring epoch is more eutrophic than the middle and contemporary epochs, indicating a

362 decline in nutrient concentrations over time. This effect is also evident in the LC core, where *Chl-*

363 *a* concentrations decreased with time and signals the entrance to the gulf of more oligotrophic

364 water during the middle and contemporary epochs. Perhaps the most notable seasonal scenario

365 occurs in the summer to early October period, when the CWF "tongue" extends in the interior of

366 the GoM. Although the concentration of *Chl-a* in the Western GoM declines gradually with time

367 to from ~ 0.09 to ~ 0.08 *mg m*$^{-3}$, the interesting fact is that the area of oligotrophic water expands

368 and become larger in the contemporary period. On the other hand, in the LC core, the *Chl-a*

369 concentrations in the three epochs do not significantly differ, suggesting that the water entering

370 the GoM is from a single source, namely, the Caribbean Sea. In general, the extensive penetration

371 of the LC within the GoM, as well as the increase in the life periods and sizes of LCEs coincide

372 with the intrusion of nutrient-poor CW.

373   Two points summarize the result of the seasonal analysis of the three epochs: First, the

374 extent of the CW intrusion confirms the north-west migration of eddies during each epoch, second,

375 the *Chl-a* concentration declines over time.

376   The second point was confirmed by calculating the average *Chl-a* concentrations outside

377   the continental shelf over two time periods, considering only the concentrations above waters

378   deeper than 250 *m*. Using data from 1998 to 2002 (SeaWIFS), and from 2009 to 2014 (MODIS)

379   we conducted a student-t test for difference in the means (Fig. 10). The latter period was

380   significantly lower with t = 4.75 and p<0.001 (n_1 = 1,825; n_2 = 2,190). This analysis confirms that

381   the *Chl-a* concentration of the GoM decreases over time and appears to disagree with the results

382   of Müller-Karger et al. (2015) who did not indicate a time trend in *Chl-a* concentration in the GoM.

383   As the data were taken with different sensors and to eliminate the uncertainty that this difference

384   is not caused by a systematic difference between the SeaWIFS and MODIS data sets used in our

385   analysis, we calculated least square regressions to the SeaWIFS and MODIS time series at four

386   stations corresponding to the northwest, northeast, southwest and southeast regions of Müller-

387   Karger et al. (2015) (Fig. 11). For each data set, inner slopes as well as overall slopes were

388   calculated. For all four stations, the SeaWIFS (1998-2002) and the MODIS (2003-2017) data series

389   merged exactly and all stations show negative trends; equivalently, the combined time series

390   (1998-2017) also show a negative tendency, supporting the conclusion that the *Chl-a*

391   concentrations over the deep GoM has decreased over time.

392   The difference between our results and those obtained by Müller-Karger et al. (2015) may

393   be attributed to the different way in which in this work and treated the data. Müller-Karger et al.

394   (2015) divided the GoM into 4 quadrants with depths of over 1000 m: Region 1-North East (RO1),

395   Region 2 (RO2 -Northwest), Region 3 (RO3-Southeast), and Region 4 (RO4 Southwest) and

396   calculated the spatial average in each quadrant to build four-time series, from 1993 to 2012. In

397   their words, "Time series of anomalies of wind speed, SST, SSHA and *Chl-a* concentration were

398   obtained by subtracting the monthly mean (climatology) from the monthly field for that variable".

399   Time series of wind speed, sea surface temperature (SST), sea-surface height (SSH), and *Chl-a*

400   data obtained at these stations from satellite products was analyzed statistically, and plotted. Other

401   variables plotted by Müller-Karger et al. (2015) were mixed layer depth (MLD) as calculated from

402   a hydrodynamic model, and net primary production (NPP) calculated from MODIS data using the

403   vertically generalized productivity model (VGPM) of Behrenfeld and Falkowski (1997).

404   On the other hand, we calculated the average of the *Chl-a* concentration pixel by pixel in

405   waters over 250 m depth, for two time periods (1998-2002 and 2009-2014), and subtracted the

406   respective monthly (climatological) means to find the difference (Fig. 10). From 2009 onward, the

407   difference indicated a small reduction of *Chl-a* in the first optical depth (1-20 or 40 meters of

408   depth) that is increasing with time. A student-t test was used to conclude that the reduction was

409   significant. We also treated the data exactly as did and Müller-Karger et al. (2015) obtained slightly

410   negative slopes Müller-Karger et al. (2015) over the entire 1998 to 2013 period.

411   We suggest that Müller-Karger et al. (2015) did not detect the small negative trend in their

412   *Chl-a* plots because their calculated slopes indicated no time-dependent change. We surmise that

413   they were also influenced by the lack of slope in the modeled MLD plot, despite clear, positive,

414   trends for SST, SSHA, and wind force. Actually, although close to zero, the slopes, as indicated

415   in Müller-Karger et al. (2015) were not zero, but -0.03 for RO1, -0.01 for RO2, and simply given

416   in as -0.0 for RO3 and 0.0 for RO4 (see their Table 1). Müller-Karger et al. (2015) also ignored

417   the fact that the time-*Chl-a* correlation coefficients (R) for all four regions was negative.

418   To confirm our findings, we chose 4 stations, each one centrally located in each quadrant

419   (Müller-Karger et al., 2015), and conducted regression analyses of the logarithmic transform of

420   the SeaWifs and MODIS *Chl-a* concentrations. All four regions showed a negative slope, a

421   negative R, and the negative slopes in the southern gulf (RO3 and RO4) were significantly different

422   from 0 ($p \ll 0.05$). This is shown in Fig. 11.

423   The observed small, but persistent decline in *Chl-a* from 1993 to 2017 may be attributed

424   to the AMOC's over-all effect of warming the surface water and thereby promoting stratification.

425   However, we wish to make clear that our conclusion about the recent time-dependent lowering of

426   the *Chl-a* pertains only to the near surface, and may not indicate a decrease in the primary

427   productivity integrated over the entire water column. In the GoM, the chlorophyll maximum as

428   measured by fluorescence occurs at about 75 m, e.g., below one optical depth, and is greater in

429   summer than in winter (Pasqueron de Fommervault et al.*,* 2017), indicating that the relationship

430   between water column productivity and near surface *Chl-a* concentration in the GoM requires

431   further study. Our own results and conclusions are based on SeaWifs and AquaMODIS chlorophyll

432   data, which in Type One water**,** correlate very well with chlorophyll measured with standard

433   laboratory methods (Mati Kahru, personal communication). In our work we can only say that

434   according to these satellite products, we find a time-dependent diminution of the Chl-a signal. This

435   diminution has been widely observed by others although in other waters (Behrenfeld et al., 2006,

436   Polovina et al., 2008; Irwin and Oliver, 2009, Laffoley and Baxter., 2016).

437

438   **4. Summary and conclusions**

439   The availability of a large spatial extension of satellite observations of ADT, sea surface currents,

440   wind stress over a quarter of century and Chl-a over 20 years has enabled us to confirm the LC

441   and CW dynamics observed in the 60's and 70's with more recent *in situ* observations. The

442   verification of the CWF climatologies developed in this work is important as a reference baseline

443   for further numerical modeling, and it impacts assessments of the gulf's biogeochemistry, energy,

444   heat transport, and Chl-a concentration. A recent committee of the National Academic of Sciences,

445   (2018) suggested three main study topics to advance the knowledge of the processes that

446 characterize the GoM: 1) the LC system active area, 2) the variation of the inflows of the LC

447 system, and 3) the dynamic interactions of the LC system in the west. Following these suggestions,

448 we have confirmed that the maximum influence of the CW into the GoM (e,g., its maximum

449 extension into the gulf or intrusion) has a temporal variability, being stronger in summer and

450 weaker in the late fall and winter. This is supported by the fact that the generated monthly EKE

451 maps have the maximum gradient at the periphery of the CWF and have a similar monthly pattern

452 of extension and retraction as the CWF.

453   We noted that in the summer months the wind stress from the southeast is weak, thereby

454 minimizing the flow of nutrients to the surface and causing Chl-a to be low, specifically for three

455 reasons: 1) The increase in the surface temperature of the water column strengthens stratification

456 2) The intrusion of the CW to the western gulf´s surface thickens the surface layer, and 3) The

457 eddy-driven anticyclonic circulation deepens the nutricline. This contrasts with the cold seasons,

458 when the surface temperature of the water is lower and the northerly winds are stronger, favoring

459 the flow of nutrients to the surface.

460   The three-year running averages of ADT 40 cm isoline reproduce qualitatively the

461 climatological pattern of a quarter of a century showing that before 2002 the CWF was less

462 intrusive and the LCEs sizes were smaller. In the 1993-2002 period, we calculated that the mean

463 life cycle of the eddies was 6.8 months and that in the 2003-2015 period the mean life cycle was

464 11.7 months. This difference suggests that after 2003, larger volumes of oligotrophic waters from

465 Caribbean Sea have invaded the western GoM and reduced mean surface Chl-a concentrations.

466 This work shows that

467   • The intrusion of the CW by LC-LCEs extends further into the western GoM than was

468   previously known.

469   • *Chl-a* concentrations respond to the dynamics inside the GoM and are influenced by

470   the CWF and the LC anticyclonic and cyclonic eddies.

471   • Since 2002, near surface *Chl-a* concentrations over bathymetry deeper than 250 m

472   have decreased, and GoM surface waters may be turning more oligotrophic than in the

473   previous decade.

474   This work, based on 25 years of remotely sensed data, emphasizes the role of climatology

475   in determining GoM circulation and its productivity and suggests that further climatologically-

476   induced changes are probably imminent.

477

478   **5. Acknowledgements**

479   This study was carried out as part of the PhD thesis research conducted by the lead author at the

480   Faculty of Marine Science and the Oceanographic Research Institute (FCM-IIO / UABC),

481   Postgraduate Coastal Oceanography Program, and it was supported by the Graduate Professional

482   Development Mexican Program grants (PRODEP: DSA/103.5/16/5801), the National Institute of

483   Technology of Mexico (TecNM) and the Mexican Energy Bureau and Hydrocarbons Mexican

484   Trust, project 201441. This is a contribution of the Gulf of Mexico Research Consortium (CIGoM).

485

486   **6. References**

487   Aguirre-Gómez, R. and Salmerón-García, O.: Characterization of the western Caribbean Sea

488   waters through in vivo chlorophyll fluorescence, Rev. Mar. Cost., 7, 9–26,

489 https://doi.org/10.15359/revmar.7.1, 2015.

490

491 Austin, G. B.: Some recent oceanographic surveys of the Gulf of Mexico, EOS, Transactions

492 American Geophysical Union, 36(5), 885-892, https://doi.org/10.1029/TR036i005p00885, 1955.

493

494 Badan, A., Candela, J., Sheinbaum, J., and Ochoa, J.: Upper-layer circulation in the approaches to

495 Yucatan Channel. In: W. Sturges and A. Lugo-Fernandez (Eds.), New Developments in the

496 Circulation of the Gulf of Mexico, Geophysical Monograph Series, 161, 57-69, 2005.

497

498 Baker-Yeboah, S., Byrne, D. A., and Watts, D. R.: Observations of mesoscale eddies in the South

499 Atlantic Cape Basin: Baroclinic and deep barotropic eddy variability, Journal of Geophysical

500 Research, 115, C12069, https://doi.org/10.1029/2010JC006236, 2010.

501

502 Behrenfeld, M. J., and Falkowski, P. G.: Photosynthetic rates derived from satellite-based

503 chlorophyll concentration, Limnology and Oceanography, 42(1), 1-20, 1997.

504

505 Behrenfeld, M. J., O'Malley, R. T., Siegel, D. A., McClain, C. R., Sarmiento, J. L., Feldman, G.

506 C., … Boss, E. S.: Climate-driven trends in contemporary ocean productivity. Nature, 444(7120),

507 752–755. https://doi.org/10.1038/nature05317, 2006.

508

509 Behringer, D. W., Molinari, R. L., and Festa, J. F.: The Variability of Anticyclonic Current Patterns

510 in the Gulf of Mexico, Journal of Geophysical Research, 82(34), 5469-5476,

511 https://doi.org/10.1029/JC082i034p05469, 1977.

512

513 Boyer, J. N., Kelble, C. R., Ortner, P. B., and Rudnick, D. T.: Phytoplankton bloom status:

514 Chlorophyll- a biomass as an indicator of water quality condition in the southern estuaries of

515 Florida,   USA,   Ecological   Indicators,   9(6),   S56–S67,

516 https://doi.org/10.1016/j.ecolind.2008.11.013, 2009.

517

518 Brown, O. B., Olson, D. B., Brown, J. W., and Evans, R. H.: Satellite infrared observations of the

519 kinematics of a warm-core ring, Marine and Freshwater Research, 34(4), 535-545,

520 https://doi.org/10.1071/MF9830535, 1983.

521

522 Bunge, L., Ochoa, J., Badan, A., Candela, J., and Sheinbaum J.: Deep flows in the Yucatan

523 Channel and their relation to changes in the Loop Current extension, Journal of Geophysical

524 Research, 107(C12), 1–7, https://doi.org/10.1029/2001JC001256, 2002.

525

526 Candela, J., Ochoa, J., Sheinbaum, J., López, M., Pérez-Brunius, P., Tenreiro, M., … Arriaza-

527 Oliveros, L.: The Flow through the Gulf of Mexico. Journal of Physical Oceanography, 49(6),

528 1381–1401. https://doi.org/10.1175/JPO-D-18-0189.1, 2019.

529

530 Candela, J., Sheinbaum, J., Ochoa, J., Badan, A., and Leben, R.: The potential vorticity flux

531 through the Yucatan Channel and the Loop Current in the Gulf of Mexico, Geophysical Research

532 Letters, 29(22), 2059, https://doi.org/10.1029/2002GL015587, 2002.

533

534 Candela, J., Tanahara, S., Crepon, M., Barnier, B., and Sheinbaum, J.: Yucatan Channel flow:

535   Observations versus CLIPPER ATL6 and MERCATOR PAM models, Journal of Geophysical

536   Research: Oceans, 108(C12), 3385, https://doi.org/10.1029/2003JC001961, 2003.

537

538   Cardona, Y., and Bracco, A.: Predictability of mesoscale circulation throughout the water column

539   in the Gulf of Mexico, Deep Sea Research Part II: Topical Studies in Oceanography, 129, 332-

540   349, https://doi.org/10.1016/j.dsr2.2014.01.008, 2016.

541

542   Chang, Y. L., and Oey, L. Y.: Why does the Loop Current tend to shed more eddies in summer

543   and winter? Geophysical Research Letters, 39(5), 1–7. https://doi.org/10.1029/2011GL050773,

544   2012.

545

546   Chang, Y.-L., and Oey, L.-Y.: Eddy and Wind-Forced Heat Transports in the Gulf of Mexico.

547   Journal of Physical Oceanography, 40(12), 2728–2742. https://doi.org/10.1175/2010JPO4474.1,

548   2010.

549

550   Chang, Y.-L., and Oey, L.-Y.: Loop Current Growth and Eddy Shedding Using Models and

551   Observations: Numerical Process Experiments and Satellite Altimetry Data. Journal of Physical

552   Oceanography, 43(3), 669–689. https://doi.org/10.1175/JPO-D-12-0139.1, 2013.

553

554   Counillon, F., and Bertino, L.: High-resolution ensemble forecasting for the Gulf of Mexico eddies

555   and fronts, Ocean Dynamics, 59(1), 83–95, https://doi.org/10.1007/s10236-008-0167-0, 2009.

556

557   Damien, P., Pasqueron de Fommervault, O., Sheinbaum, J., Jouanno, J., Camacho-Ibar, V. F., and

558 Duteil, O.: Partitioning of the Open Waters of the Gulf of Mexico Based on the Seasonal and

559 Interannual Variability of Chlorophyll Concentration, Journal of Geophysical Research: Oceans

560 (March), 1–23, https://doi.org/10.1002/2017JC013456, 2018.

561

562 Dandonneau, Y., Deschamps, P. Y., Nicolas, J. M., Loisel, H., Blanchot, J., Montel, Y., Thieuleux,

563 F., and Bécu, G.: Seasonal and interannual variability of ocean color and composition of

564 phytoplankton communities in the North Atlantic, equatorial Pacific and South Pacific, Deep Sea

565 Research Part II: Tropical Studies in Oceanography, 51(1–3), 303–318,

566 https://doi:10.1016/j.dsr2.2003.07.018, 2004.

567

568 de Ruijter, W. P.M., Biastoch, A., Drijfhout, S. S., Lutjeharms, J. R. E., Matano, R. P., Pichevin,

569 T., van Leeuwen, P. J., and Weijer, W.: Indian-Atlantic interocean exchange: Dynamics,

570 estimation and impact, Journal of Geophysical Research: Oceans, 104(C9), 20885-20910,

571 https://doi.org/10.1029/1998jc900099, 1999.

572

573 Fowler, J., Cohen, L., and Jarvis, P.: Practical statistics for field biology, John Wiley & Sons, 2013.

574

575 Fratantoni, P. S., Lee, T. N., Podesta, G. P., and Müller-Karger, F.: The influence of Loop Current

576 perturbations on the formation and evolution of Tortugas eddies in the southern Straits of Florida,

577 Journal of Geophysical Research: Oceans, 103(C11), 24759-24779,

578 https://doi.org/10.1029/98JC02147, 1998.

579

580 Garcia-Jove, M., Sheinbaum, J., and Jouanno J.: Sensitivity of Loop Current metrics and eddy

581 detachments to different model configurations: The impact of topography and Caribbean

582 perturbations, Atmosfera, 29(3), 235–265, https://doi.org/10.20937/ATM.2016.29.03.05, 2016.

583

584 Goni, G. J., and Johns, W. E.: A census of North Brazil Current rings observed from

585 TOPEX/POSEIDON altimetry: 1992–1998, Geophysical Research Letters, 28(1), 1-4,

586 https://doi.org/10.1029/2000GL011717, 2001.

587

588 Hall, C. A., and Leben, R. R.: Observational evidence of seasonality in the timing of loop current

589 eddy separation. Dynamics of Atmospheres and Oceans, 76, 240–267.

590 https://doi.org/10.1016/j.dynatmoce.2016.06.002, 2016.

591

592 Hamilton, P., Lugo-Fernández, A., and Sheinbaum, J.: A Loop Current experiment: Field and

593 remote measurements, Dynamics of Atmospheres and Oceans, 76, 156-173,

594 https://doi.org/10.1016/j.dynatmoce.2016.01.005, 2016.

595

596 Huh, O. K., Wiseman, W. J. J., and Rouse, L. J.: Intrusion of loop current waters onto the West

597 Florida continental shelf, Journal of Geophysical Research, 86(C5), 4186–4192,

598 https://doi.org/10.1029/JC086iC05p04186, 1981.

599

600 Hall, C. R. and Leben, R.R., 2016. Observational Evidence of Seasonality in the timing of Loop

601 Current eddy separation, Dynamics of Atmosphere and Oceans 76,240-367.

602

603 Hurlburt, H. E., and Thompson, J. D.: A numerical study of loop current intrusions and eddy

604 shedding, Journal Physical Oceanography, 10(10), 1611–1651, https://doi.org/10.1175/1520-

605 0485(1980)010<1611:ansolc>2.0.co;2, 1980.

606

607 Irwin, A. J., and Oliver, M. J.: Are ocean deserts getting larger? Geophysical Research Letters,

608 36(18), L18609. https://doi.org/10.1029/2009GL039883, 2009.

609

610 Jouanno, J., Sheinbaum Pardo, J., Barnier, B., Molines, J. M., and Candela Pérez, J.: Seasonal and

611 interannual modulation of the Eddy Kinetic Energy in the Caribbean Sea, Journal of Physical

612 Oceanography, 42(11), 2041-2055. doi: 10.1175/JPO-D-12-048.1, 2012.

613

614 Jouanno, J., Sheinbaum, J., Barnier B., and Molines, J. M.: The mesoscale variability in the

615 Caribbean Sea. Part II: Energy sources, Ocean Modelling., 26(3–4), 226–239,

616 https://doi.org/10.1016/j.ocemod.2008.10.006, 2009.

617

618 Laffoley, D., and Baxter, J. M.: Explaining Ocean Warming: Causes, scale, effects and

619 consequences, Full Report. Gland, Switzerland: IUCN, 27,

620 https://doi.org/10.2305/IUCN.CH.2016.08.en, 2016.

621

622 Leben, R. R.: Altimetry-derived Loop Current metrics, In Circulation of the Gulf of Mexico:

623 Observations and Models, Geophysical Monograph Series, 161, edited by W. Sturges, and A.

624 Lugo-Fernandes, pp. 181–201, AGU, Washington, D. C., 2005.

625

626 Leben, R. R., and Born, G. H.: Tracking Loop Current eddies with satellite altimetry, Advances in

627 Space Research, 13(11), 325-333, https://doi.org/10.1016/0273-1177(93)90235-4,1993.

628 Leipper, D. F.: A sequence of current patterns in the Gulf of Mexico, Journal of Geophysical

629 Research, 75(3), 637-657, https://doi.org/10.1029/JC075i003p00637, 1970.

630

631 Lindo-Atichati, D., Bringas, F., and Goni, G.: Loop Current excursions and ring detachments

632 during 1993-2009, International Journal of Remote Sensing, 34(14), 5042–5053,

633 https://doi.org/10.1080/01431161.2013.787504, 2013.

634

635 Liu, Y., Lee, S.-K., Muhling, B. A., Lamkin, J. T., and Enfield, D. B.: Significant reduction of the

636 Loop Current in the 21st century and its impact on the Gulf of Mexico, Journal of Geophysical

637 Research, 117, C05039, https://doi.org/10.1029/2011JC007555, 2012.

638

639 Martínez-López, B., and Zavala-Hidalgo, J.: Seasonal and interannual variability of cross-shelf

640 transports of chlorophyll in the Gulf of Mexico, Journal of Marine Systems, 77(1–2), 1–20,

641 https://doi.org/10.1016/j.jmarsys.2008.10.002, 2009.

642

643 Maul, G. A., and Vukovich, F. M.: The relationship between variations in the Gulf of Mexico Loop

644 Current and Straits of Florida Volume Transport, Journal of Physical Oceanography, 23(5), 785–

645 796, https://doi.org/10.1175/1520-0485(1993)023<0785:TRBVIT>2.0.CO;2, 1993.

646

647 Molinari, R. L., Baig, S., Behringer, D. W., Maul, G. A., and Legeckis, R.: Winter intrusions of

648 the Loop Current, Science, 198(4316), 505-507, https://doi.org/10.1126/science.198.4316.505,

649 1977.

650   Morrison, J. M., Merrell Jr, W. J., Key, R. M., and Key, T. C.: Property distributions and deep

651   chemical measurements within the western Gulf of Mexico. Journal of Geophysical Research:

652   Oceans, 88(C4), 2601-2608. https://doi.org/10.1029/JC088iC04p02601, 1983.

653

654   Müller-Karger, F. E., McClain, C. R., Fisher, T. R., Esaias, W. E., and Varela, R.: Pigment

655   distribution in the Caribbean Sea: Observations from space, Progress in Oceanography, 23(1), 23-

656   64, https://doi.org/10.1016/0079-6611(89)90024-4, 1989.

657

658   Müller-Karger, F. E., Smith, J. P., Werner, S., Chen, R., Roffer, M., Liu, Y., Muhling, B., Lindo-

659   Atichati, D., Lamkin, J., Cerdeira-Estrada, S., and Enfield, D.B.: Natural variability of surface

660   oceanographic conditions in the offshore Gulf of Mexico, Progress in Oceanography 134:54-76,

661   https://doi.org/10.1016/j.pocean.2014.12.007, 2015.

662

663   Müller-Karger, F. E., Walsh, J. J., Evans, R. H., and Meyers, M. B.: On the seasonal phytoplankton

664   concentration and sea surface temperature cycles of the Gulf of Mexico as determined by satellites,

665   Journal of Geophysical Research, 96(C7), 12645, https://doi.org/10.1029/91JC00787, 1991.

666

667   National Academies of Sciences, Engineering, and Medicine: Understanding and Predicting the

668   Gulf of Mexico Loop Current: Critical Gaps and Recommendations, Washington, DC: The

669   National Academies Press, https://doi.org/10.17226/24823, 2018.

670

671   Niiler, P. P.: Observations of low-frequency currents on the West Florida continental shelf,

672   Memoires Societé Royale des Sciences de Liege, 6, 331-358, 1976.

673   Nof, D.: The momentum imbalance paradox revisited, Journal of Physical Oceanography, 35(10),

674   1928-1939, https://doi.org/10.1175/JPO2772.1, 2005.

675

676   Nowlin, W. D., and McLellan, H. J.: A characterization of Gulf of Mexico waters in winter, Journal

677   of Marine Research, 25(1), 29-59, 1967.

678

679   Oey, L.-Y.: Effects of winds and Caribbean eddies on the frequency of Loop Current eddy

680   shedding: A numerical model study, Journal of Geophysical Research, 108(C10), 1–25,

681   https://doi.org/10.1029/2002JC001698, 2003.

682

683   Oey, L.-Y., Ezer, T., Forristall, G., Cooper, C., DiMarco, S., and Fan, S.: An exercise in forecasting

684   loop current and eddy frontal positions in the Gulf of Mexico, Geophysical Research. Letters,

685   32(12), L12611, https://doi.org/10.1029/2005GL023253, 2005.

686

687   Paluszkiewicz, T., Atkinson, L. P., Posmentier, E. S., and McClain, C. R.: Observations of a Loop

688   Current frontal eddy intrusion onto the West Florida Shelf, Journal of Geophysical Research:

689   Oceans, 88(C14), 9639-9651, https://doi.org/10.1029/JC088iC14p09639,1983.

690

691   Pasqueron de Fommervault, O., Perez-Brunius, P., Damien, P., and Sheinbaum, J.: Temporal

692   variability of chlorophyll distribution in the Gulf of Mexico: bio-optical data from profiling floats,

693   Biogeosciences, 14, 5647-5662, https://doi.org/10.5194/bg-14-5647-2017, 2017.

694

695   Pichevin, T., and Nof, D.: The momentum imbalance paradox, Tellus, Series A: Dynamic

696   Meteorology Oceanography, 49(2), 298–319, https://doi.org/10.3402/tellusa.v49i2.14484, 1997.

697

698   Pichevin, T., Nof, D., and Lutjeharms, J.: Why are there Agulhas rings?, Journal of Physical

699   Oceanography,   29(4),   693-707,   https://doi.org/10.1175/1520-

700   0485(1999)029<0693:WATAR>2.0.CO;2, 1999.

701

702   Polovina, J. J., Howell, E. A., and Abecassis, M.: Ocean's least productive waters are expanding,

703   Geophysical Research Letters, 35(3), 2–6, https://doi.org/10.1029/2007GL031745, 2008.

704

705   Portela, E., Tenreiro, M., Pallàs-Sanz, E., Meunier, T., Ruiz-Angulo, A., Sosa-Gutiérrez, R., and

706   Cusí, S.: Hydrography of the Central and Western Gulf of Mexico. Journal of Geophysical

707   Research: Oceans, 123(8), 5134–5149. https://doi.org/10.1029/2018JC013813, 2018.

708

709   Richardson, P. L.: Eddy kinetic energy in the North Atlantic from surface drifters, Journal of

710   Geophysical Research: Oceans, 88(C7), 4355-4367, https://doi.org/10.1029/JC088iC07p04355,

711   1983.

712

713   Savidge, D. K., and Bane, J. M.: Cyclogenesis in the deep ocean beneath the Gulf Stream. I-

714   Description, Journal of Geophysical Research, 104, 18, https://doi.org/10.1029/1999JC900132,

715   1999.

716

717   Schmitz, W. J.: Cyclones and westward propagation in the shedding of anticyclonic rings from the

718   Loop Current, In Circulation in the Gulf of Mexico: Observations and Models, Geophysical

719 Monograph Series, 161, 241–262, https://doi.org/10.1029/161GM18, 2005.

720

721 Schmitz, W. J., Jr., Biggs, D. C., Lugo-Fernandez, A., Oey, L.-Y., and Sturges, W.: A synopsis of

722 the circulation in the Gulf of Mexico and on its continental margins. In Circulation in the Gulf of

723 Mexico: Observations and Models, Geophysical Monograph Series, 161, 11–30,

724 https://doi.org/10.1029/161GM03, 2005.

725

726 Schmitz, W. J., Jr., and McCartney, M. S.: On the North Atlantic circulation, Reviews of

727 Geophysics, 31(1), 29–50, https://doi.org/10.1029/92RG02583, 1993.

728

729 Sturges, W. and Lugo-Fernandez, A.: Circulation in the Gulf of Mexico: Observations and Models,

730 Geophysical Monograph Series, 161, 347 pp. https://doi.org/10.1029/GM161, 2005

731

732 Sudre, J., Maes, C., and Garcon, V.: On the global estimates of geostrophic and Ekman surface

733 currents, Limnology and Oceanography: Fluids and Environments, 3, 1–20,

734 https://doi.org/10.1215/21573689-2071927, 2013.

735

736 Vukovich, F. M.: Loop Current boundary variations, Journal of Geophysical Research, Oceans,

737 93(C12), 15,585-15,591, https://doi.org/10.1029/JC093iC12p15585, 1988.

738

739 Vukovich, F. M., Crissman, B. W., Bushnell, M., and King, W. J.: Some aspects of the

740 oceanography of the Gulf of Mexico using satellite and in situ data, Journal of Geophysical

741 Research, 84, 7749, https://doi.org/10.1029/JC084iC12p07749, 1979.

742   Wei, M., Jacobs, G., Rowley, C., Barron, C. N., Hogan, P., Spence, P.,... & Coelho, E.: The

743   performance of the US Navy's RELO ensemble, NCOM, HYCOM during the period of GLAD at-

744   sea experiment in the Gulf of Mexico. Deep Sea Research Part II: Topical Studies in

745   Oceanography, 129, 374-393, https://doi.org/10.1016/j.dsr2.2013.09.002, 2016.

746

747   Zavala-Hidalgo, J., Morey, S. L., and O'Brien, J. J.: Cyclonic Eddies Northeast of the Campeche

748   Bank from Altimetry Data, Journal oh Physical Oceanography, 33(3), 623–629,

749   https://doi.org/10.1175/1520-0485(2003)033<0623:CENOTC>2.0.CO;2, 2003.

750

751   Zavala-Hidalgo, J., Morey, S. L., O'Brien, J. J., and Zamudio, L.: On the Loop Current eddy

752   shedding variability, Atmosfera, 19(1), 41–48, 2006.

753

754   Zeng, X., Li, Y., and He, R.: Predictability of the loop current variation and eddy shedding process

755   in the Gulf of Mexico using an artificial neural network approach, Journal of Atmospheric and

756   Oceanic Technology, 32(5), 1098-1111, https://doi.org/10.1175/JTECH-D-14-00176.1, 2015.

757

758   Zharkov, V., and Nof, D.: Why Does the North Brazil Current Regularly Shed Rings but the Brazil

759   Current Does Not?, Journal of Physical Oceanography, 40(2), 354-367,

760   https://doi.org/10.1175/2009JPO4246.1, 2010.

761
762
763

764 Table 1. Average bold numbers for *Chl-a* concentrations (*mg m^{-3}*) and differences (*mg m^{-3}*; (%)) between
765 Early and Contemporary averages at two geographical areas: 95.5°W, 22.12°N and 91.5°W, 25.87°N,
766 (Western GoM) and 86°W, 22.12°N and 84.75°W, 23.37°N (LC-LCEs) during "**early**" (1998-2002), "**middle**"
767 (2003-2008), and "**contemporary**" (2009-2014) epochs. Table 1 shows the compared averages in bold
768 print. Standard deviations and number of pixels considered are shown in parenthesis.

Geographical Areas	Season	Early Averages (1998-2002)	Middle Averages (2003-2008)	Contemp. Averages (2009-2014)	Difference (Early-Contemp)
Western GoM	Winter	**0.180** (±0.047, n=4026)	**0.167** (±0.048, n=4866)	**0.173** (±0.0624, n=4828)	**0.007 (4%)**
Loop Current		**0.149** (±0.052, n=536)	**0.129** (±0.064, n=647)	**0.117** (±0.062, n=645)	**0.032 (21%)**
Western GoM	Spring	**0.114** (±0.033, n=3693)	**0.087** (±0.049, n=4658)	**0.0834** (±0.036, n=4754)	**0.030 (27%)**
Loop Current		**0.0948** (±0.074, n=526)	**0.085** (±0.1287, n=642)	**0.0835** (±0.116, n=648)	**0.011 (12%)**
Western GoM	Summer	**0.0887**(±0.024, n=3924)	**0.080** (±0.022, n=4794)	**0.0755** (±0.023, n=4837)	**0.013 (15%)**
Loop Current		**0.109** (±0.217, n=535)	**0.091** (±0.171, n=647)	**0.0938** (±0.148, n=648)	**0.015 (14%)**
Western GoM	Autumn	**0.151** (±0.052, n=3894)	**0.137** (±0.044, n=4876)	**0.127** (±0.043, n=4846)	**0.024 (16%)**
Loop Current		**0.138** (±0.128, n=525)	**0.1325** (±0.114, n=643)	**0.122** (±0.103, n=648)	**0.016 (12%)**

769

FIGURE CAPTIONS:

Fig. 1. Monthly means of absolute dynamic topography (ADT) and surface currents averaged over a quarter of a century (1993-2017).

Fig. 2. Climatological monthly maps of eddy kinetic energy (EKE) in GoM: red color contours correspond to the areas of maxima EKE. The heavy black line corresponds to the isoline of 40 *cm* 2.2 *cm* of the CWF (the contour of the CWF is significant at the 95% of level). The EKE was calculated using daily maps of satellite-derived currents from AVISO (GEKCO) for a quarter of a century (1993 – 2017).

Fig. 3. Geographical positions of the CWF tracked using the 40 *cm* ADT isoline representing 1993-2017 monthly average values: a) Northward and b) Westward, respectively; c) ADT spectral analysis in a region influenced by the CWF (91.25ºW, 23.125ºN and 83.5ºW, 28.12ºN).

Fig. 4. The ADT quarter-century CWF (1993-2017) monthly climatology and its standard deviation are shown in heavy and dotted lines, respectively. The heavy line corresponds to the 40 *cm* isoline of the CWF. The dotted line encloses values of the standard deviation >15 *cm*.

Fig. 5. Average monthly percentage surface areas of CW in the interior of the Gulf of Mexico determined from climatology of the STD contour > 15 *cm*; enclosed areas were calculated in relation to the GoM area ($1.56 \times 10^6 \ km^2$).

Fig. 6. Monthly means of absolute dynamic topography (ADT) from 1993-2002 (color) and its respective CWF computed with the 40 *cm* isoline (heavy black line).

Fig. 7. Monthly means of absolute dynamic topography (ADT) from 2003-2017 (color) and respective CWF computed with the 40 *cm* isoline (heavy black line).

Fig. 8. Monthly climatologies of *Chl-a* (SeaWIFS, 1998-2002 and MODIS data source, 2003-2017). The heavy black line represents the contour of the 40 *cm* ADT data that represents the CWF (1998-2017). *Chl-a* values larger than 1 *mg m^{-3}* are plotted in red.

Fig. 9. From top left to bottom right, average *Chl-a* values according to period: column 1, SeaWIFS 1998-2002, column 2, MODIS 2003-2008, and column 3, MODIS 2009-2014. From top to bottom figures correspond to the mean seasons. Average *Chl-a* concentration is computed inside the white and red squares (white corresponds to the western GoM and red corresponds to the LC area). Average values for each time period and season are in Table 1.

Fig. 10. Differences of *Chl-a* concentration (*mg m^{-3}*) between 2009-2014 average values of MODIS data minus 1998-2002 average SeaWIFS values. The broken line represents the 250 *m* isobath. White contoured areas indicate no significant differences.

Fig. 11. *Chl-a* concentrations (*mg m^{-3}*) at four stations (a to d) in the GoM, daily time series derived from SeaWIFS from 1998 to 2002 (green) and MODIS from 2003 to 2017 (blue). Least square regressions for SeaWIFS (red line), MODIS (cyan line), and the overall linear regressions for each station (dashed black line).

816   FIGURE 1

819   FIGURE 2

820

821

823

824

825

     FIGURE 4

ADT STD contour colors (dotted line 15 cm) & CWF (thick line 40 cm)
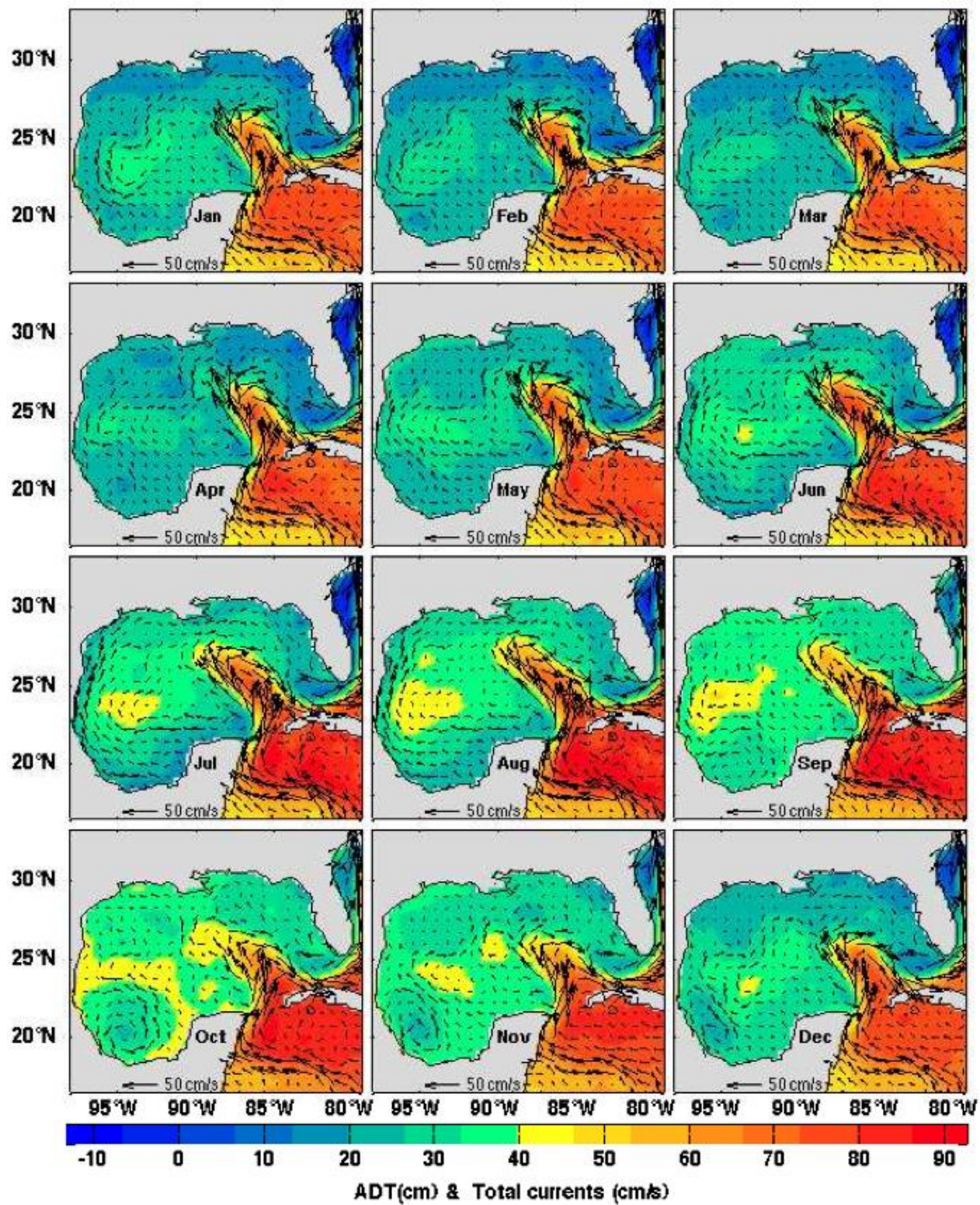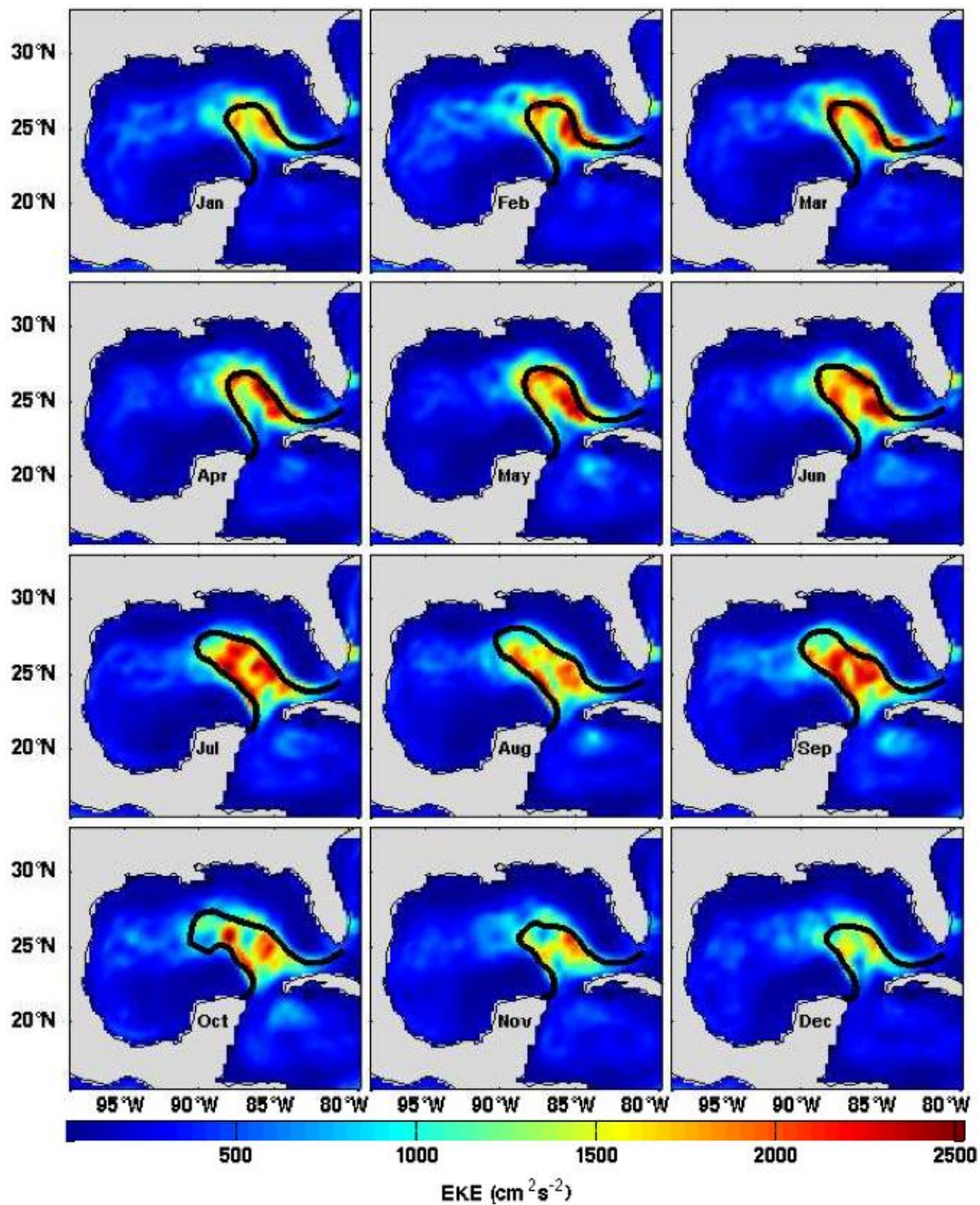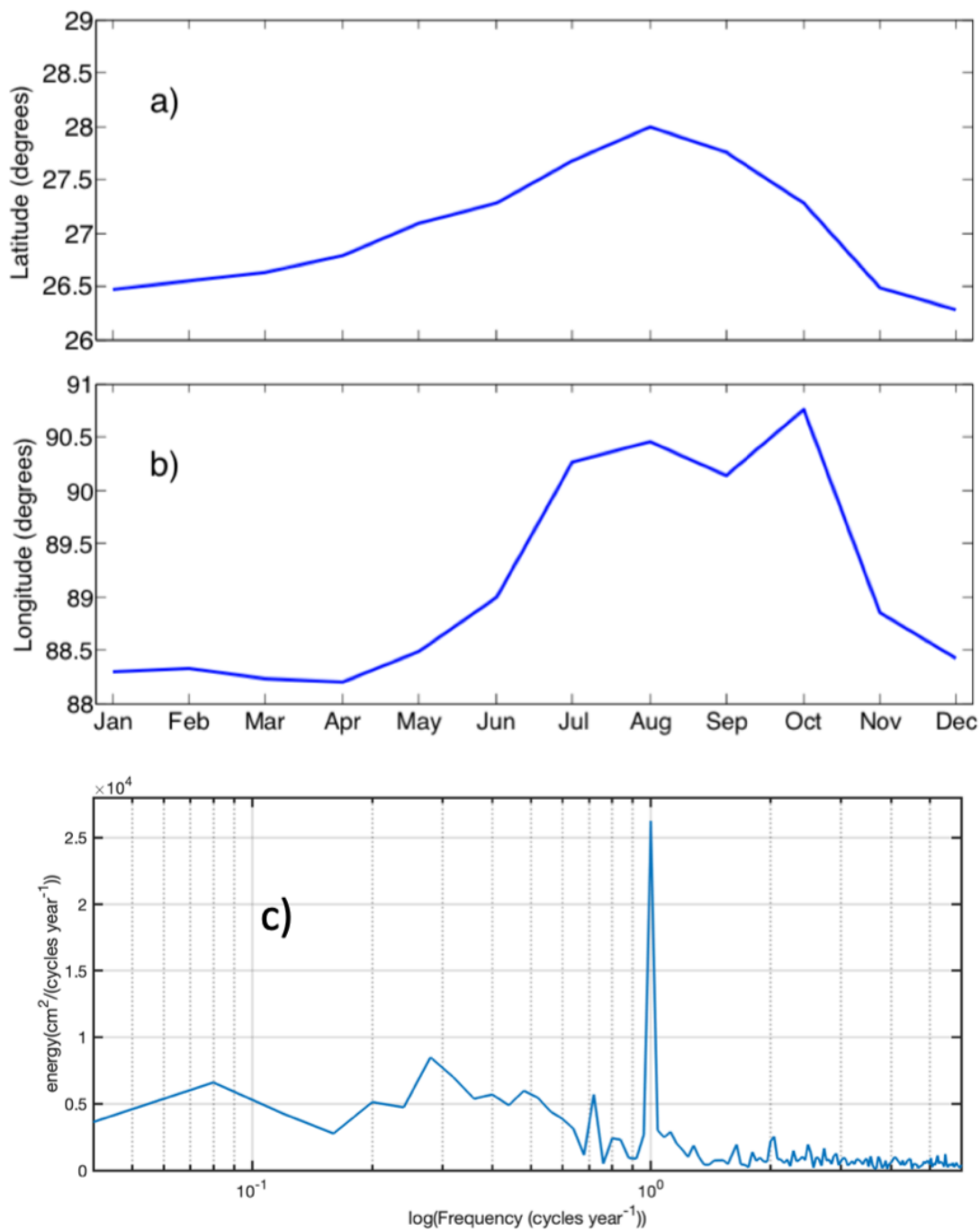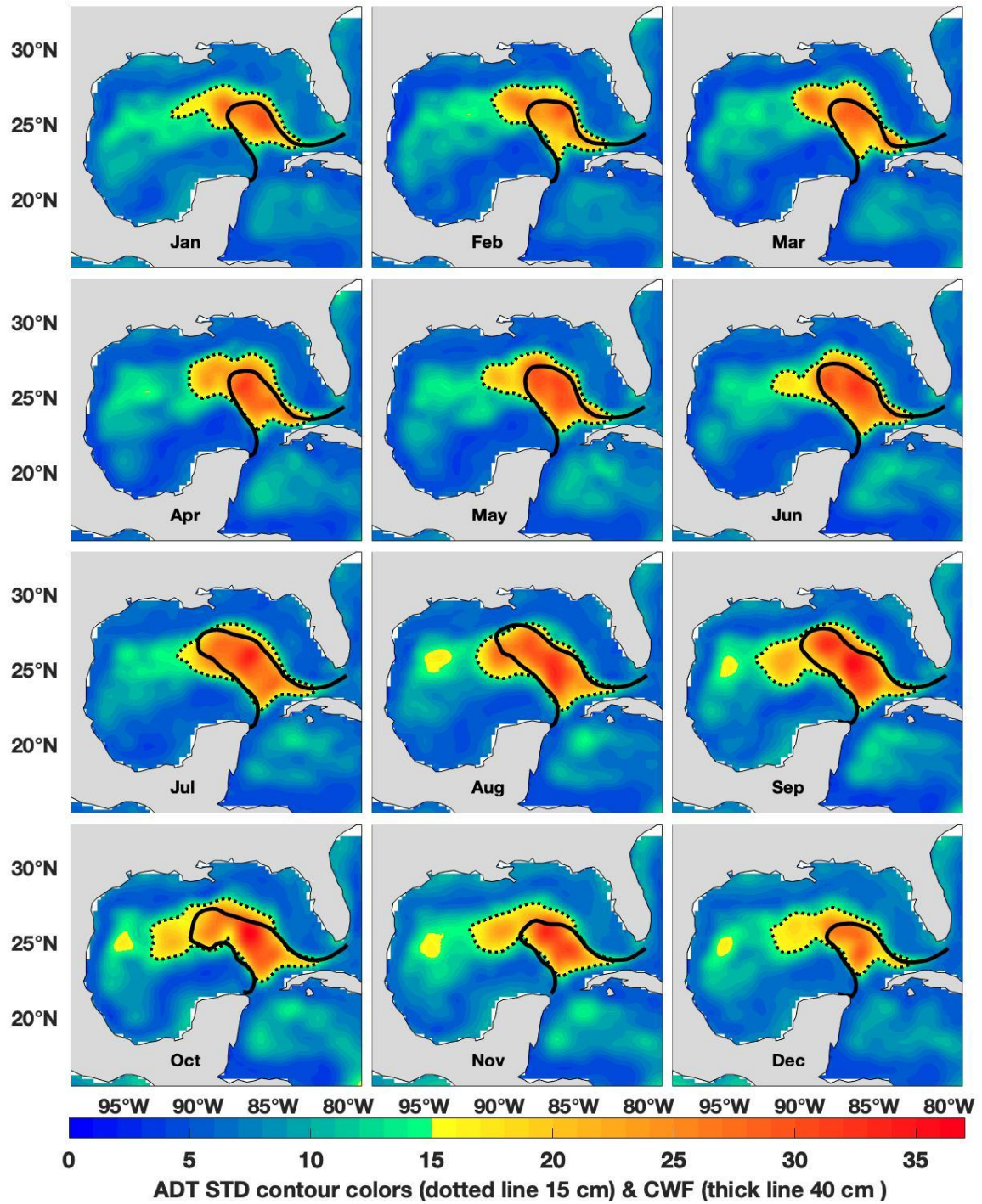
827

828

829
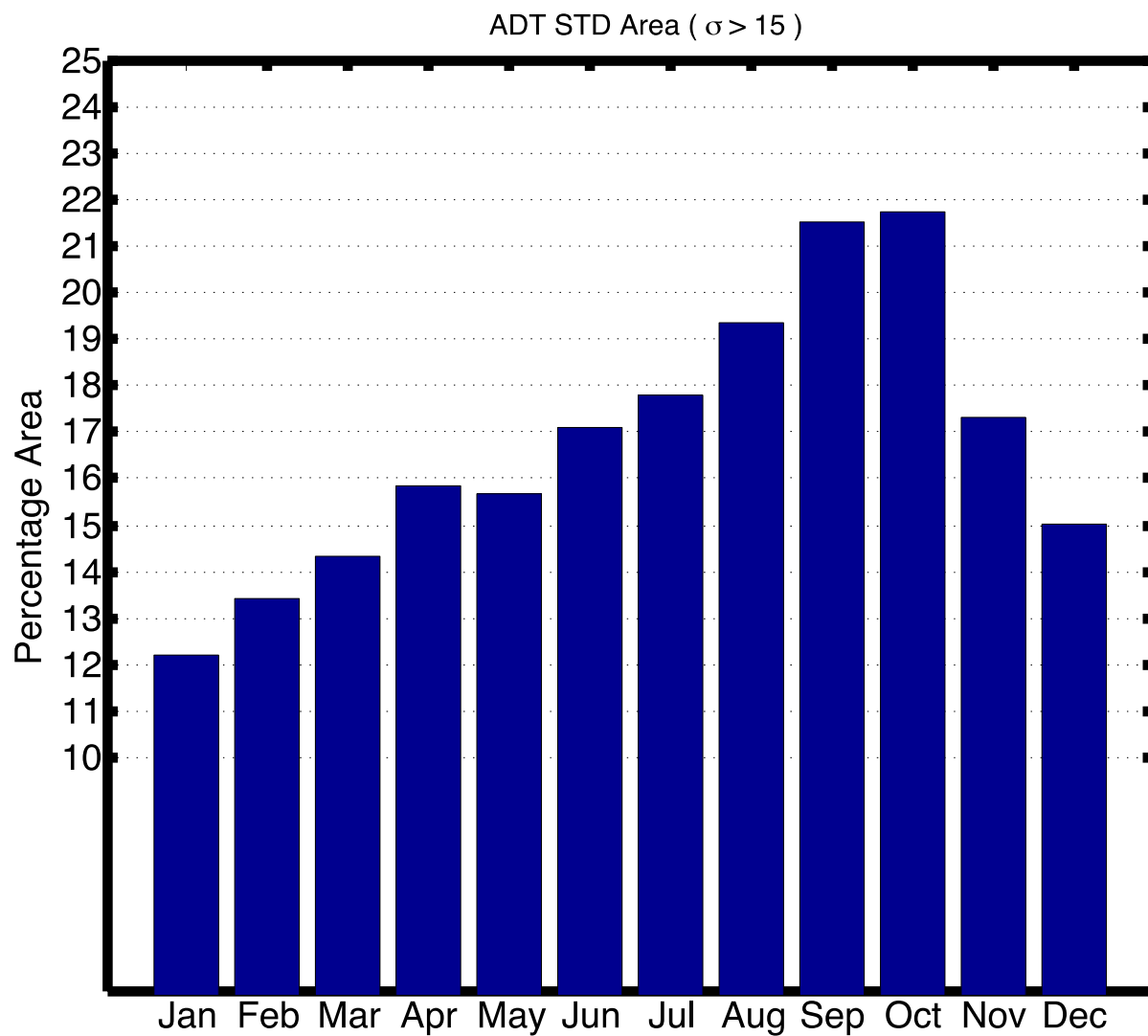
831

832

833

834

835

836

837

838

839   FIGURE 6

840

841

843

844

848   FIGURE 9

849

850

851

852   FIGURE 10

Chlorophyll difference (M20092014 - S19982002) mg m^{-3}
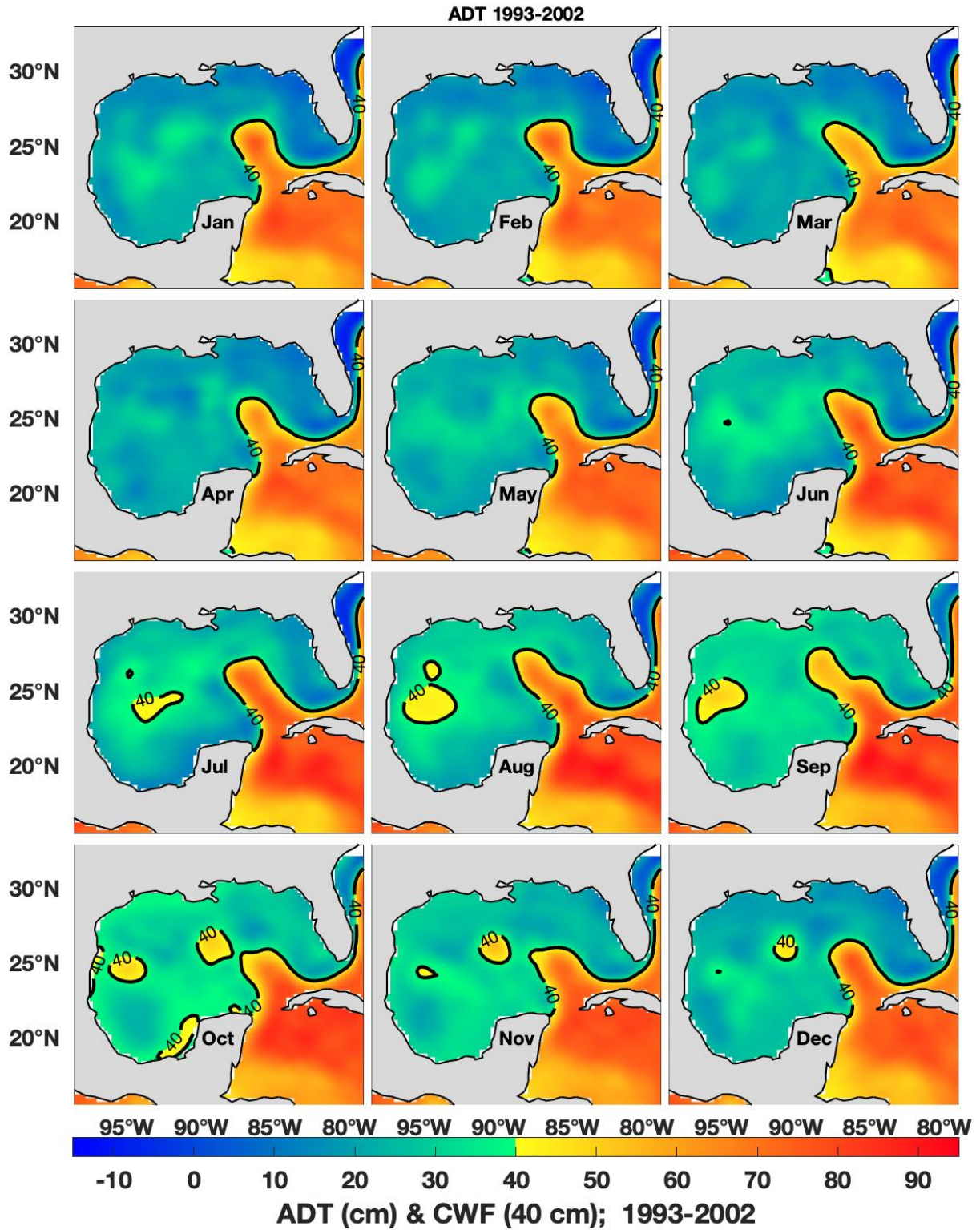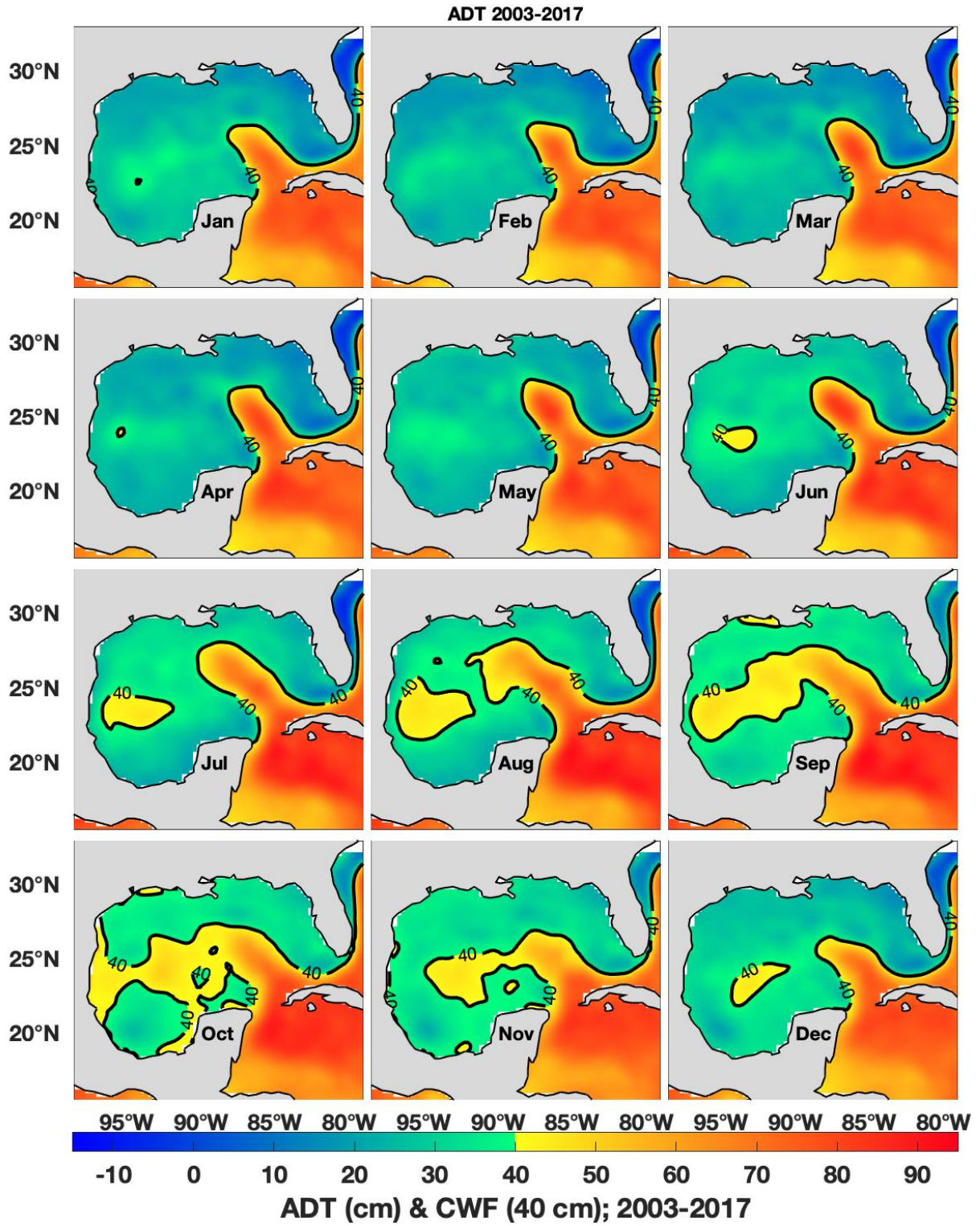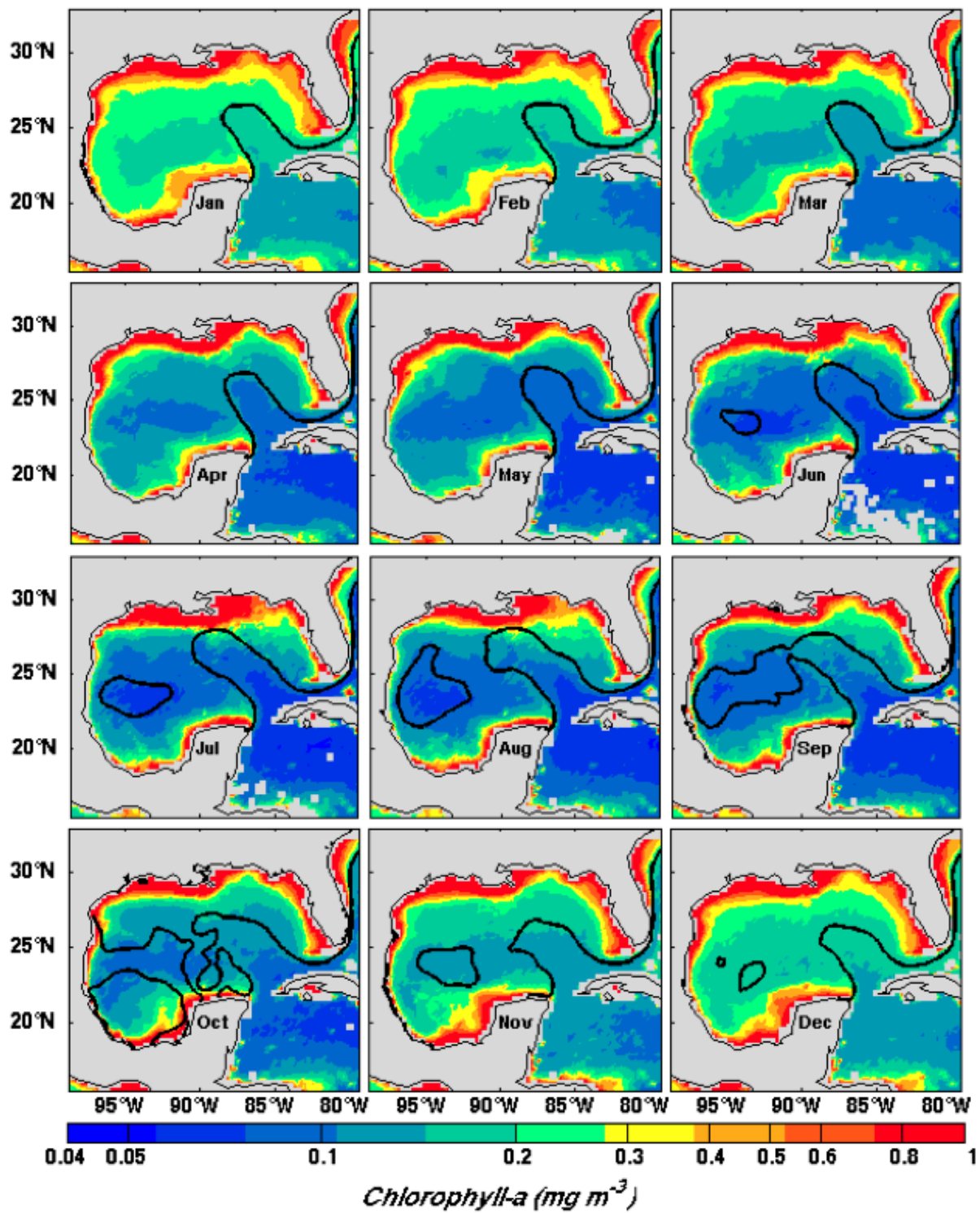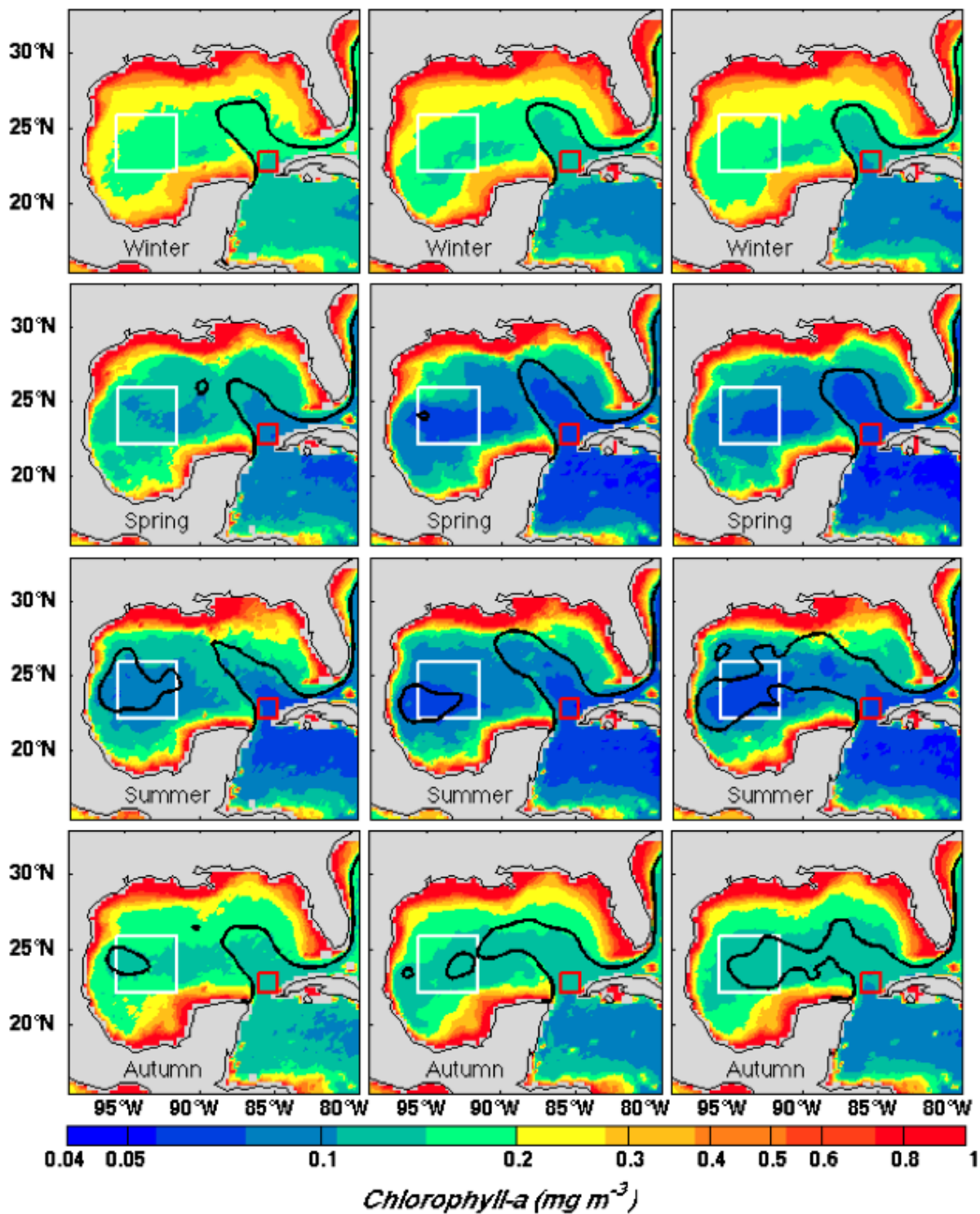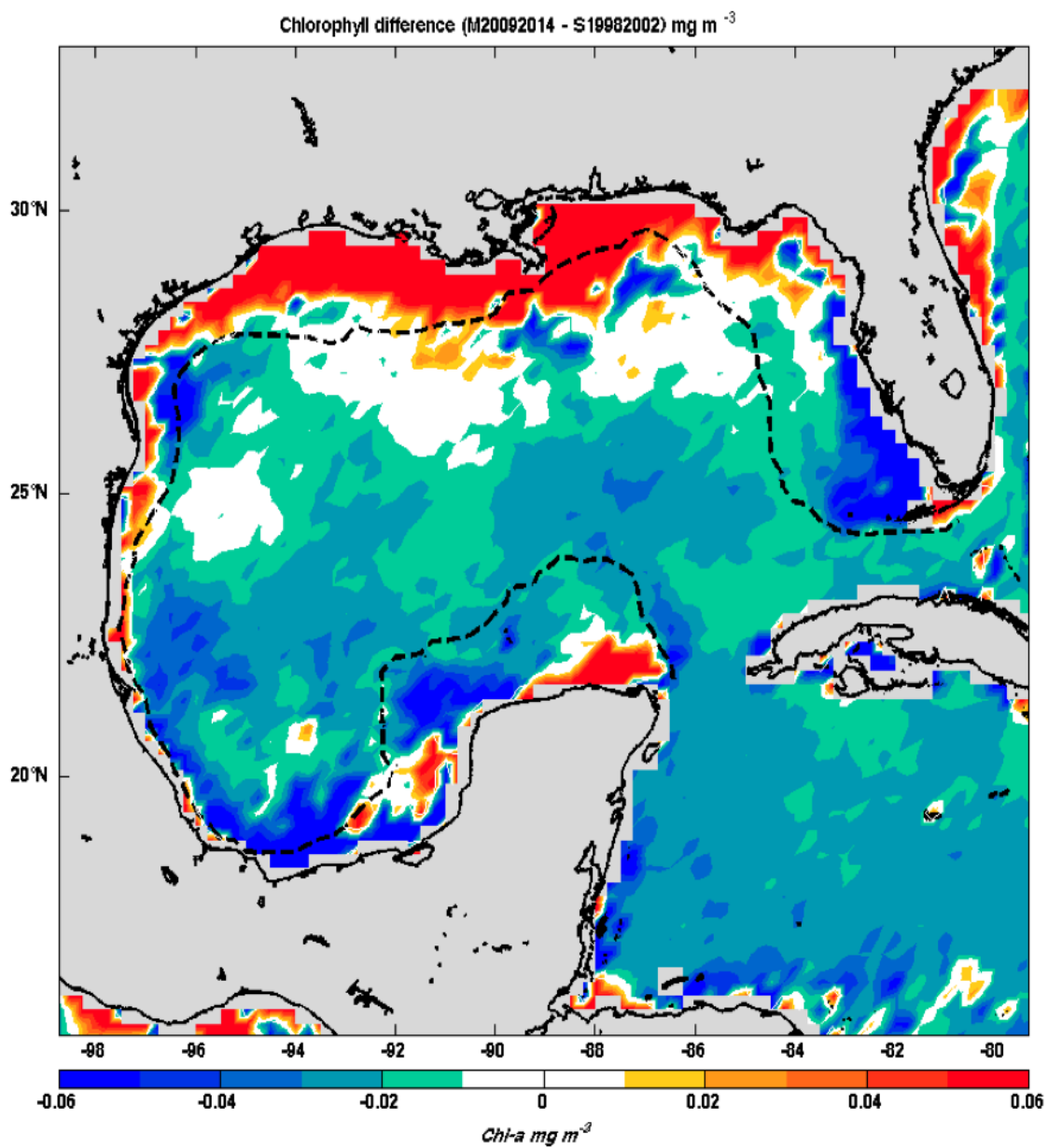
853

854

855

856

857

858

859

860   FIGURE 11

861

862

863

864

865